# Nonreciprocal Frequency Domain Beam Splitter

Nils T. Otterstrom, Shai Gertler, Eric A. Kittlaus, Michael Gehl, Andrew L. Starbuck, Christina M. Dallo, Andrew T. Pomerene, Douglas C. Trotter, Peter T. Rakich, Paul S. Davids, and Anthony L. Lentine

Phys. Rev. Lett. **127**, 253603 — Published 15 December 2021

DOI: 10.1103/PhysRevLett.127.253603

# A nonreciprocal frequency domain beam splitter

Nils T. Otterstrom,[1,*] Shai Gertler,[2] Eric A. Kittlaus,[3] Michael Gehl,[1] Andrew L. Starbuck,[1] Christina M. Dallo,[1] Andrew T. Pomerene,[1] Douglas C. Trotter,[1] Peter T. Rakich,[2] Paul S. Davids,[1] and Anthony L. Lentine[1]

[1] *Photonic and Phononic Microsystems, Sandia National Laboratories, Albuquerque, New Mexico 87185, USA*
[2] *Department of Applied Physics, Yale University, New Haven, CT 06520 USA.*
[3] *Jet Propulsion Laboratory, California Institute of Technology, Pasadena, CA 91109 USA.*

(Dated: October 28, 2021)

The canonical beam splitter—a fundamental building block of quantum optical systems—is a reciprocal element. It operates on forward- and backward-propagating modes in the same way, regardless of direction. The concept of nonreciprocal quantum photonic operations, by contrast, could be used to transform quantum states in a momentum- and direction-selective fashion. Here we demonstrate the basis for such a nonreciprocal transformation in the frequency domain through inter-modal Bragg scattering four-wave mixing (BSFWM). Since the total number of idler and signal photons is conserved, the process can preserve coherence of quantum optical states, functioning as a nonreciprocal frequency beam splitter. We explore the origin of this nonreciprocity and find that the phase-matching requirements of inter-modal BSFWM produce an enormous asymmetry (76×) in the conversion bandwidths for forward and backward configurations, yielding $\sim 25$ dB of nonreciprocal contrast over several hundred GHz. We also outline how the demonstrated efficiencies ($\sim 10^{-4}$) may be scaled to near unity values with readily accessible powers and pumping configurations for applications in integrated quantum photonics.

## INTRODUCTION

Noiseless unitary operations may be used to transform quantum states while preserving their coherence. In this context, photonic-based quantum information processing relies on the ability to control and manipulate the quantum degrees of freedom of light—its path, polarization, frequency, momentum, etc—without degrading its quantum coherence [1–3]. As many quantum-optics applications move to the chip scale, mature techniques for phase delay, polarization rotation, and switching have enabled complex quantum information processing systems and protocols in integrated photonic circuits [4–7]. So far, however, the manipulations used in these demonstrations have primarily been reciprocal; a switch, for instance, routes counter-propagating light along the exact same path traced out by forward propagating light. The advent of new on-chip nonreciprocal technologies [8–17] raises important considerations and opportunities at the particular intersection we call nonreciprocal quantum photonics [18–24]. Nonreciprocal operations may find an important role in mitigating some forms of intersymbol interference, a phenomenon that can potentially degrade the fidelity of both classical [25] and quantum networks [26, 27]. Moreover, the ability to achieve dynamically controlled nonreciprocal operations that can operate at the few and single-photon levels may be used to protect delicate quantum systems from unwanted noise and interference [28, 29] and enable direction-dependent logic for quantum architectures [19, 29–31].

The frequency of light is one of the most useful degrees of freedom for quantum applications [32]. Manipulating a photon's frequency has historically been achieved through traditional nonlinear optical operations such as second harmonic generation [33] or parametric down conversion [34], which in general require a $\chi^{(2)}$ medium [35]. In the leading silicon-based integrated photonics platforms, however, $\chi^{(2)}$ nonlinearities are not naturally present, requiring artificial $\chi^{(2)}$ effects [36–38] or recourse to $\chi^{(3)}$ nonlinearities [35]. In particular, a powerful $\chi^{(3)}$ nonlinear frequency conversion technique called Bragg scattering four-wave mixing (BSFWM)—amenable to an array of integrated photonic and fiber-based systems [39–44]—exhibits dynamics that intrinsically add no quantum noise [45]. In contrast to other four wave mixing (FWM) processes, such as non-degenerate FWM, that amplify vacuum fluctuations, this frequency translation process preserves quantum coherence because the total signal and idler photon number is conserved [45]. In this way, BSFWM can be viewed as a beam splitter in the frequency domain for quantum states [41, 45]. In this nonlinear optical process, it has been suggested that the phase-matching conditions and the directionality of the pump fields may give rise to a form of optical nonreciprocity [46]. However, the actual nonreciprocal response associated with the BSFWM frequency conversion process has not been demonstrated or explored. Understanding and leveraging these conditions is a first step towards low-loss nonreciprocal frequency translation of photonic states for quantum information processing.

In this Letter, we use inter-modal BSFWM to demonstrate nonreciprocal frequency conversion—the frequency analogue of a nonreciprocal beam splitter—for the first time. We leverage modal degrees of freedom within low-loss silicon ridge waveguides to precisely control and clearly demonstrate the phase-matching properties of this form of frequency conversion. This allows us to perform mode and direction-specific frequency conversion. We find a 76× asymmetry in the phase-matching bandwidths for forward and backward-oriented frequency conversion processes, enabling $\sim 25$ dB of nonreciprocal contrast over $\sim 3$ nm. The results indicate that high-efficiency and broad-bandwidth nonreciprocal frequency conversion is within reach in standard silicon photonic circuits, opening the door to nonreciprocal frequency beam splitter operations for new functionalities in quantum photonics.

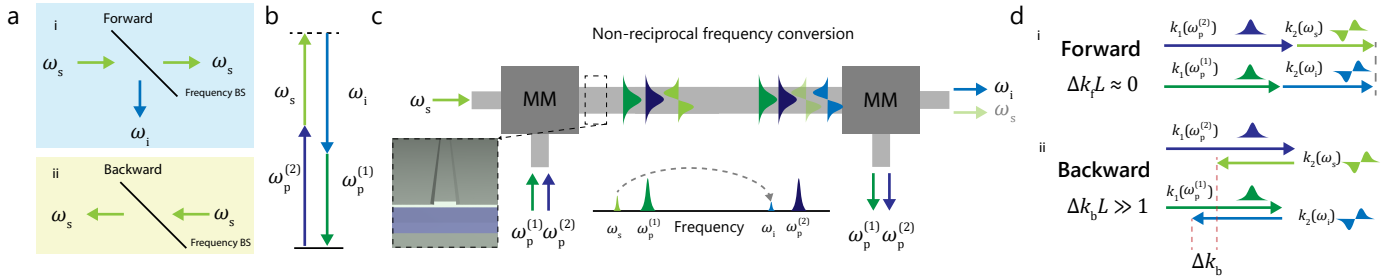


FIG. 1. (a) Basic operation of a nonreciprocal frequency beam splitter. (ai) In the forward direction, a signal wave is split into both signal and idler modes. (aii) In the backward direction, by contrast, the signal is transmitted without splitting into the idler mode. (b) Energy conservation for BSFWM. (c) Implementation of nonreciprocal frequency conversion (i.e., frequency beam splitting) through inter-modal BSFWM. The schematic diagrams the operation scheme for frequency conversion in the forward direction. Pump fields (of frequencies $\omega_{\rm p}^{(1)}$ and $\omega_{\rm p}^{(2)}$, respectively) are coupled into the symmetric mode of the multimode waveguide (inset) using an integrated mode multiplexer. A signal wave, of frequency $\omega_{\rm s}$, is injected into the antisymmetric mode. As the fields traverse the nonlinear active region of the device, signal light ($\omega_{\rm s}$) is converted to the idler frequency ($\omega_{\rm i}$) through inter-modal BSFWM. Inset depicts the waveguide cross-sectional geometry. (di) Phase-matching for inter-modal BSFWM in the forward direction. The sum of wavevectors from the signal and pump 2 fields must equal the corresponding sum for the idler and pump 1 fields within the phase-matching uncertainty $\Delta k_{\rm f}$. (dii) Backward inter-modal BSFWM precluded by phase-matching. If $\omega_{\rm p}^{(2)}$ is outside the narrow phase-matching bandwidth, there is a nonreciprocal phase-mismatch given by $\Delta k_{\rm b}$, and light in the counter-propagating signal wave does not experience frequency conversion to the idler frequency ($\omega_{\rm i}$).

## RESULTS

We use a form of BSFWM-based frequency conversion to produce nonreciprocal beam splitting in the frequency domain. The essential device physics can be understood diagrammatically as depicted in Fig. 1a. Through this process, a forward-propagating input signal wave is split into output signal and idler modes, with a splitting ratio given by the efficiency of the BSFWM frequency conversion process. In the backward direction, by contrast, the signal wave remains in the signal frequency mode.

We demonstrate BSFWM-based frequency conversion within a multimode silicon ridge waveguide that supports symmetric and antisymmetric TE-like optical spatial modes, with wavevectors described by the dispersion relations $k_1(\omega)$ and $k_2(\omega)$, respectively. With these two modal degrees of freedom, we can precisely shape the phase-matching constraints imposed by Bragg-scattering four wave mixing to (1) avoid deleterious noise-inducing $\chi^{(3)}$ effects and (2) achieve nonreciprocal frequency conversion over a desired, well-defined bandwidth.

Bragg scattering four wave mixing can be leveraged to translate classical and quantum states of light between distinct frequencies without intrinsically adding noise. Fig. 1c depicts the particular implementation of BSFWM for frequency conversion that we use here. In this case, BSFWM requires two strong optical fields, which we label pump 1 ($\omega_{\rm p}^{(1)}$) and pump 2 ($\omega_{\rm p}^{(2)}$), as well a signal field with frequency $\omega_{\rm s}$. Generally, the pumps are strong classical fields, in contrast to the signal field, which can be represented by either a quasi-classical or quantum state. Through this nonlinear process, a pump 2 photon ($\omega_{\rm p}^{(2)}$) and signal photon ($\omega_{\rm s}$) are annihilated to create a pump 1 photon ($\omega_{\rm p}^{(1)}$) and an idler photon ($\omega_{\rm i}$), as diagrammed in Fig. 1b-c. In contrast to other FWM phenomena, such as phase conjugation and modulation interactions, BSFWM does not produce amplification and its accompanying excess noise [45]. Rather, as diagrammed in Fig. 1a, it can be viewed as an active beam splitter where the two output modes are defined by the the signal and idler frequencies [41].

The beam splitter analogue becomes evident in the traveling-wave interaction Hamiltonian for this BSFWM process [45], which in simplified form is given by

$$H_{\rm BSFWM} = \hbar \int dz \left( \kappa a_{\rm i}^{\dagger} a_{\rm s} e^{i\Delta k z} + \kappa^* a_{\rm i} a_{\rm s}^{\dagger} e^{-i\Delta k z} \right), \qquad (1)$$

where $a_{\rm i}$ and $a_{\rm s}$ represent annihilation operators of the idler and signal fields, respectively, $\kappa$ quantifies the degree of coupling from BSFWM, $\Delta k$ is the phase-mismatch given by $\Delta k = k_{\rm s} + k_{\rm p}^{(2)} - k_{\rm i} - k_{\rm p}^{(1)}$. Taking into account these interactions as well as the interaction Hamiltonian for self- and cross-phase modulation effects (see detailed derivation in Supplementary Section I, which includes Refs. [45, 47, 48]), we find the spatial equations of motion for the signal and idler fields given by

$$\begin{aligned} \partial_z a_{\rm s} &= i\delta\beta a_{\rm s} - i\kappa a_{\rm i}, \\ \partial_z a_{\rm i} &= -i\delta\beta a_{\rm i} - i\kappa^* a_{\rm s}, \end{aligned} \qquad (2)$$

where $\kappa = 2\gamma_{12}\sqrt{P_{\rm p}^{(1)} P_{\rm p}^{(2)}}$ and $\delta\beta = \frac{1}{2}\Delta k + \frac{1}{2}\gamma_{11}(P_{\rm p}^{(2)} - P_{\rm p}^{(1)})$, and $\gamma_{11}$ and $\gamma_{12}$ are the intra- and inter-modal Kerr coefficients, and we have assumed strong coherent pump fields of powers $P_{\rm p}^{(1,2)}$. We note that for simplicity we have moved to the spatial rotating frame and treated the pump fields as undepleted.

These equations have spatial solutions given by [45]

$$\begin{aligned} a_{\rm s}(z) &= \bar{\mu}(z) a_{\rm s}(0) + \bar{v}(z) a_{\rm i}(0) \\ a_{\rm i}(z) &= -\bar{v}^*(z) a_{\rm s}(0) + \bar{\mu}^*(z) a_{\rm i}(0), \end{aligned} \qquad (3)$$

where $\bar{\mu}(z)$ and $\bar{v}(z)$ are given by $\bar{\mu}(z) = \cos(qz) + (i\delta\beta/2q)\sin(qz)$ and $\bar{v}(z) = (i\kappa/q)\sin(qz)$, and $q$ is defined

by $q = (|\kappa|^2 + \delta\beta^2)^{1/2}$. The crucial role of phase-matching appears in the scattering efficiency given by

$$\begin{aligned} |\bar{v}(z)|^2 &= |\kappa|^2 \frac{\sin^2([\delta\beta^2 + |\kappa|^2]^{1/2} z)}{[\delta\beta^2 + |\kappa|^2]} \\ &\approx |\kappa|^2 z^2 \mathrm{sinc}^2(\Delta k z/2) \end{aligned} \tag{4}$$

for small Kerr couplings.

These conditions produce an intriguing form of phase-matching induced nonreciprocity. For the form of inter-modal BSFWM demonstrated here, energy conservation and phase matching conditions require that for a finite interaction length $L$ and for a signal wave frequency detuned by $\Omega$ from pump 1 ($\omega_\mathrm{s} = \omega_\mathrm{p}^{(1)} - \Omega$),

$$\begin{aligned} \Delta k L = &|(\bar{k}_1(\omega_\mathrm{p}^{(2)}) + \bar{k}_2(\omega_\mathrm{p}^{(1)} - \Omega) \\ &- \bar{k}_1(\omega_\mathrm{p}^{(1)}) - \bar{k}_2(\omega_\mathrm{p}^{(2)} - \Omega)| L \\ &< 2.78, \end{aligned} \tag{5}$$

where the bars denote the vector nature of the wavevectors, and 2.78 gives the full width at half maximum (FWHM) of a $\mathrm{sinc}^2$. Neglecting higher order dispersion, this relation yields a phase-matching bandwidth ($\Delta\omega = \omega_\mathrm{p}^{(2)} - \omega_\mathrm{p}^{(1)}$) that is given by

$$\Delta\omega = \frac{2.78}{L|\frac{1}{\bar{v}_{\mathrm{g},1}} - \frac{1}{\bar{v}_{\mathrm{g},2}}|}. \tag{6}$$

We note here that the vector nature of the group velocities $\bar{v}_{\mathrm{g},1}$ and $\bar{v}_{\mathrm{g},1}$ plays a critical role in determining the phase-matching bandwidth. For typical multimode waveguides the group velocity difference between two modes is relatively small, yielding a very broad phase matching bandwidth for frequency conversion in the co-propagating configuration given by

$$\Delta\omega_\mathrm{f} = \frac{2.78c}{L}|\frac{1}{n_{\mathrm{g},1} - n_{\mathrm{g},2}}|. \tag{7}$$

By contrast, however, this same bandwidth shrinks dramatically ($\sim 100\times$) when considering the case in which signal and idler fields counter-propagate with respect to the pump waves. In this case, the backward inter-modal BSFWM phase matching is given by

$$\Delta\omega_\mathrm{b} = \frac{2.78c}{L}|\frac{1}{n_{\mathrm{g},1} + n_{\mathrm{g},2}}|, \tag{8}$$

revealing that the phase-matching bandwidth is inherently nonreciprocal. Thus for a wide range of wavelengths, signal photons can experience the frequency conversion only in the forward direction. For instance, an incoming single signal photon and vacuum idler field (defined by $|1,0\rangle_\mathrm{in}$) spatially evolves in the Heisenberg picture as [45]

$$|1,0\rangle_\mathrm{in} = \bar{\mu}(z)|1,0\rangle_\mathrm{out} - \bar{v}^*(z)|0,1\rangle_\mathrm{out}. \tag{9}$$

When operating at conditions where the process is phase-matched in the forward direction, but not in the backward direction (i.e., $\Delta\omega_\mathrm{b} < \Delta\omega < \Delta\omega_\mathrm{f}$), we will have $\bar{v}(z) \neq 0$ in the forward direction and $\bar{v}(z) = 0$ in the backwards direction, resulting in a nonreciprocal quantum frequency beamsplitter.

## EXPERIMENTAL RESULTS

We demonstrate and explore the nonreciprocal properties of inter-modal BSFWM in a multimode silicon waveguide through heterodyne-based nonlinear spectroscopy. The waveguides measure 1.5 μm in width and support two, low-loss (< 0.5 dB/cm) TE-like optical modes with wavevectors $k_1(\omega)$ and $k_2(\omega)$, respectively. Devices are fabricated using a standard CMOS photolithography process at Sandia's MESA facilities. Nonlinear optical spectroscopy on a waveguide of length $L = 7$ mm is performed using the experimental apparatus diagrammed in Fig. 2a. Light for pumps 1 and 2 are derived from distinct tunable lasers of frequencies $\omega_\mathrm{p}^{(1)}$ and $\omega_\mathrm{p}^{(2)}$, respectively. The power of these fields is controlled by an erbium-doped fiber amplifier (EDFA) and variable optical attenuator (VOA), and these fields are subsequently injected into the symmetric mode of a multimode silicon waveguide through a grating coupler and mode multiplexer. We use an intensity modulator to synthesize a signal wave with a frequency detuning of $\Omega/2\pi = 10$ GHz ($\omega_\mathrm{s} = \omega_\mathrm{p}^{(1)} - \Omega$), which we route to the antisymmetric mode of the waveguide. As the signal wave traverses the interaction region, it experiences (with some efficiency) frequency conversion to the idler frequency through inter-modal BSFWM. Idler light is detected with high SNR using a form of frequency-selective heterodyne detection. This scheme uses an optical local oscillator that is blue-shifted by $\Delta/2\pi = 44$ MHz from $\omega_\mathrm{p}^{(2)}$, such that the converted idler light produces a distinct heterodyne beat tone at $\Omega + \Delta$, independent of the frequency detuning between the two pump waves.

We first measure the frequency conversion efficiency over a range of pump powers and relative detuning, with the signal (and idler) wave oriented in the forward direction. Fig. 2b plots the data obtained from the measurements as a function of the max total power and pump 2 wavelength. The data reveal a clear $\mathrm{sinc}^2$ response, as predicted from theory (see Eq. 4). We also plot the peak efficiency, which demonstrates excellent agreement with theory. The theoretical trend assumes a Kerr coefficient of $\gamma = 45$ W$^{-1}$m$^{-1}$, matching prior simulation work [50].

This heterodyne measurement also allows us to examine the phase coherence of the BSFWM process and possible forms of deleterious noise. For instance, through thermorefractive and thermoelastic effects, thermal flucations may be imprinted on the converted idler field in the form of phase noise (similar to frequency noise in the case of a resonator [51]). From our measurements (see inset of Fig. 2c), however, we find that this phase coherence is exceptionally well preserved in our linear waveguide system, with a near resolution-bandwidth limited idler heterodyne spectrum of 1 kHz. This minute level of noise (< 1 kHz) is

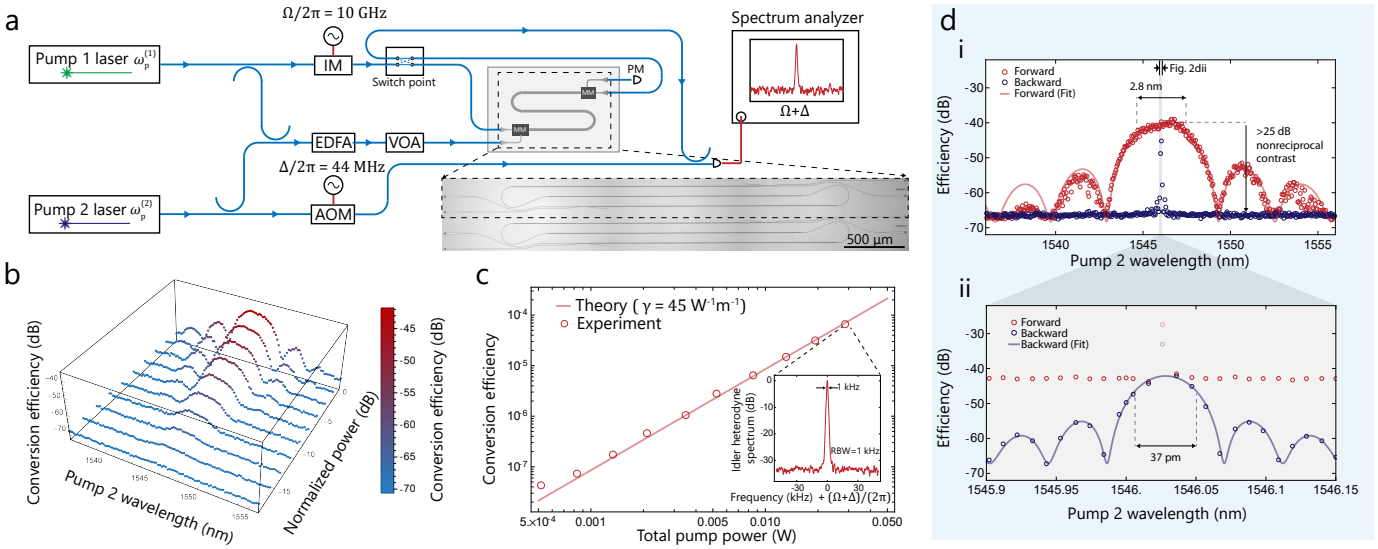


FIG. 2. Experimental apparatus for nonlinear laser spectroscopy. Laser light from the pumps ($\omega_{\mathrm{p}}^{(1)}$ and $\omega_{\mathrm{p}}^{(2)}$) are coupled together and amplified using an erbium-doped fiber amplifier (EDFA). The total power is controlled with a variable optical attenuator (VOA). Light at the signal frequency is created from pump 1 using an intensity modulator (IM) driven at $\Omega = 10$ GHz (such that $\omega_{\mathrm{s}} = \omega_{\mathrm{p}}^{(1)} - \Omega$). The signal wave is then routed into the antisymmetric mode of the multimode waveguide in either the forward or backward directions. A strong optical local oscillator for heterodyne spectroscopy is created from the pump 2 wave using an acousto-optic modulator, which blue-shifts light by $\Delta/2\pi = 44$ MHz. Combining this reference with the light exiting the antisymmetric mode yields a microwave signal at $\Omega + \Delta$ that corresponds to the generated idler wave. (b) Frequency conversion efficiency as a function of pump 2 wavelength ($\lambda_{\mathrm{p}}^{(2)} = 2\pi c/\omega_{\mathrm{p}}^{(2)}$) and combined max pump powers (normalized). (c) Peak efficiency vs total pump power, demonstrating good agreement with the theoretical trend. Inset shows the normalized idler heterodyne spectrum (averaged, near RBW-limited), demonstrating that the BSFWM process preserves the signal/idler phase coherence. The estimated on-chip signal power in these measurements is of order 5 $\mu$W. (d) Nonreciprocal frequency conversion measurements. (di) signal to idler conversion efficiency as a function of pump 2 wavelength ($\lambda_{\mathrm{p}}^{(2)} = 2\pi c/\omega_{\mathrm{p}}^{(2)}$) in the forward (red) and backward directions (dark blue), demonstrating $>$ 25 dB of nonreciprocal contrast. (dii) Backwards frequency conversion over a 76$\times$ smaller range, revealing the much tighter phase-matching constraints for backward inter-modal BSFWM. Over this range, by contrast, the forward conversion efficiency (red) is flat due to its much larger phase matching bandwidth. As such, there exist nm-wide+ spectral regions over which $\sim$ 25 dB of nonreciprocal contrast is possible. The semi-transparent data points are due to carrier-enhanced BSFWM effects (see Supplementary information of Ref. [49]) that occur only at small frequency separations of $|\omega_{\mathrm{p}}^{(1)} - \omega_{\mathrm{p}}^{(2)}| < 2\pi/\tau_{\mathrm{c}}$ ($\sim$ 1 GHz), where the free carrier lifetime $\tau_c \approx 1$ ns.

orders of magnitude smaller than the intrinsic frequency uncertainty of typical single photon wavepackets (bandwidths 1-100 GHz).

We next explore the nonreciprocal properties of the frequency conversion process. With a manual switch, this apparatus can be readily reconfigured to inject and detect signal and idler waves in the forward and backward directions. In the forward direction (see blue data points of Fig. 2di), we observe a broad sinc$^2$ phase-matching window with a bandwidth of 2.8 nm ($\sim$ 350 GHz), in good agreement with our theoretical predictions. By contrast, in the backward direction, the phase-matching bandwidth is radically reduced. Fig. 2dii presents data taken over a much narrower range, revealing a phase-matching bandwidth of 0.037 nm ($\sim$ 5 GHz), representing a 76$\times$ reduction resulting from the nonreciprocal phase-matching conditions (see Eq. 7 and Eq. 8). Outside the backward phase-matching bandwidth (but within the forward), we observe more than 25 dB of noise-floor-limited nonreciprocal contrast (see 2di).

## DISCUSSION

We have used inter-modal BSFWM to demonstrate and explore coherent nonreciprocal frequency conversion in an integrated silicon waveguide, achieving the frequency analogue of a unidirectional beam splitter. We explicitly demonstrate this nonreciprocal behavior for the first time and show that nonreciprocity arises due to the distinct phase-matching bandwidths of the forward and backward frequency conversion processes. This physics differs from prior acousto-optic nonreciprocal demonstrations wherein the optimal phase-matching for forward and backward processes is centered at distinct frequencies [9–11]. Moreover, unlike optomechanical based nonreciprocity [9–11, 13, 52], our approach—based on an all-optical nonlinearity—is not susceptible to large degrees of thermal-mechanical noise at room temperature. Furthermore, because inter-modal spontaneous four wave mixing (SFWM) is not phase-matched at these small detunings (see Supplementary Section II for more details, which includes Refs. [48, 53–56]), our particular inter-modal scheme prevents noise from parametric SFWM fluorescence that naturally occurs in conventional intra-modal

schemes [56].

An important step towards useful quantum operations is the realization of near-unity frequency conversion efficiencies. Our initial low-power continuous wave (CW) results suggest that, with accessible pump powers and device lengths, near-unity conversion efficiencies may be possible within these waveguide systems. Since the efficiency scales with optical power as $P_{\mathrm{p}}^{(1)} P_{\mathrm{p}}^{(2)}$, enhancing the pump powers by approximately 20 dB (to $\sim$ 1 W) would enhance the theoretical efficiency to near its optimal value. Such a power enhancement should be accessible using picosecond sources, which have been used to pump nonlinear processes in silicon with more than 10 W peak powers with minimal nonlinear loss or device degradation [57]. As such, moderate pulse durations ($\sim$ 100 ps) and repetition rates ($\sim$ 100 MHz) could enable Watt-level peak powers without increasing the average powers ($\sim$ 10 mW) used in this demonstration, putting unity nonreciprocal frequency conversion of single photons within reach [58].

This material is based upon work supported by the Laboratory Directed Research and Development program at Sandia National Laboratories. Sandia National Laboratories is a multi-program laboratory managed and operated by National Technology and Engineering Solutions of Sandia, LLC., a wholly owned subsidiary of Honeywell International, Inc., for the U.S. Department of Energy's National Nuclear Security Administration under contract DE-NA-0003525. This paper describes objective technical results and analysis. Any subjective views or opinions that might be expressed in the paper do not necessarily represent the views of the U.S. Department of Energy or the United States Government.

We wish to thank Ashok Kodigala for helpful discussions relating to the experimental apparatus.

* ntotter@sandia.gov

[1] M. O. Scully and M. S. Zubairy, "Quantum optics," (1999).
[2] D. F. Walls and G. J. Milburn, *Quantum optics* (Springer Science & Business Media, 2007).
[3] G. Grynberg, A. Aspect, and C. Fabre, *Introduction to quantum optics: from the semi-classical approach to quantized light* (Cambridge university press, 2010).
[4] A. Politi, J. C. Matthews, M. G. Thompson, and J. L. O'Brien, IEEE J. Sel. Top. Quant. **15**, 1673 (2009).
[5] J. W. Silverstone, J. Wang, D. Bonneau, P. Sibson, R. Santagati, C. Erven, J. O'Brien, and M. Thompson, in *2016 International Conference on Optical MEMS and Nanophotonics (OMN)* (IEEE, 2016) pp. 1–2.
[6] X. Qiang, X. Zhou, J. Wang, C. M. Wilkes, T. Loke, S. O'Gara, L. Kling, G. D. Marshall, R. Santagati, T. C. Ralph, *et al.*, Nat. Photonics **12**, 534 (2018).
[7] D. Bunandar, A. Lentine, C. Lee, H. Cai, C. M. Long, N. Boynton, N. Martinez, C. DeRose, C. Chen, M. Grein, *et al.*, Physical Review X **8**, 021009 (2018).
[8] Z. Yu and S. Fan, Appl. Phys. Lett. **94**, 171116 (2009).
[9] D. B. Sohn, S. Kim, and G. Bahl, Nat. Photonics **12**, 91 (2018).
[10] E. A. Kittlaus, W. M. Jones, P. T. Rakich, N. T. Otterstrom, R. E. Muller, and M. Rais-Zadeh, Nat. Photonics **15**, 43 (2021).
[11] E. A. Kittlaus, N. T. Otterstrom, P. Kharel, S. Gertler, and P. T. Rakich, Nat. Photonics **12**, 613 (2018).
[12] D. L. Sounas and A. Alù, Nat. Photonics **11**, 774 (2017).
[13] F. Ruesink, M.-A. Miri, A. Alu, and E. Verhagen, Nature communications **7**, 1 (2016).
[14] K. Fang, J. Luo, A. Metelmann, M. H. Matheny, F. Marquardt, A. A. Clerk, and O. Painter, Nature Physics **13**, 465 (2017).
[15] K. Wang, S. Gao, Y. Wang, A. Nirmalathas, C. Lim, K. Alameh, and E. Skafidas, IEEE Photonics Technology Letters **28**, 1739 (2016).
[16] K. Wang, Y. Wang, S. Gao, A. Nirmalathas, C. Lim, K. Alameh, H. Li, and E. Skafidas, IEEE Photonics Technology Letters **29**, 1261 (2017).
[17] S. Hua, J. Wen, X. Jiang, Q. Hua, L. Jiang, and M. Xiao, Nat. Commun. **7**, 1 (2016).
[18] D. Roy, Phys. Rev. B **81**, 155117 (2010).
[19] Y. Shen, M. Bradford, J.-T. Shen, *et al.*, Phys. Rev. Lett. **107**, 173902 (2011).
[20] L. Yuan, S. Xu, and S. Fan, Opt. Lett. **40**, 5140 (2015).
[21] K. Wang, Y. Shi, A. S. Solntsev, S. Fan, A. A. Sukhorukov, and D. N. Neshev, Opt. Lett. **42**, 1990 (2017).
[22] X.-W. Xu, A.-X. Chen, Y. Li, and Y.-x. Liu, Phys. Rev. A **96**, 053853 (2017).
[23] L. Tian and Z. Li, Phys. Rev. A **96**, 013808 (2017).
[24] M.-X. Dong, Y.-C. Yu, Y.-H. Ye, W.-H. Zhang, E.-Z. Li, L. Zeng, G.-C. Guo, D.-S. Ding, and B.-S. Shi, arXiv preprint arXiv:1908.09242 (2019).
[25] J. Kilmer and B. A. Mortimer, in *Tests, Measurements, and Characterization of Electro-Optic Devices and Systems*, Vol. 1180 (International Society for Optics and Photonics, 1990) pp. 2–9.
[26] I. Choi, R. J. Young, and P. D. Townsend, Opt. Express **18**, 9600 (2010).
[27] X. Tang, R. Kumar, D. Cunningham, A. Wonfor, R. Penty, and I. White, in *IEEE GC Wkshps* (IEEE, 2018) pp. 1–4.
[28] L.-M. Duan and H. Kimble, Phys. Rev. Lett. **92**, 127902 (2004).
[29] E. J. Lenferink, G. Wei, and N. P. Stern, Opt. Express **22**, 16099 (2014).
[30] I. Söllner, S. Mahmoodian, S. L. Hansen, L. Midolo, A. Javadi, G. Kiršanskė, T. Pregnolato, H. El-Ella, E. H. Lee, J. D. Song, *et al.*, Nat. Nanotechnol. **10**, 775 (2015).
[31] C. Gonzalez-Ballestero, E. Moreno, F. J. Garcia-Vidal, and A. Gonzalez-Tudela, Phys. Rev. A **94**, 063817 (2016).
[32] J. M. Lukens and P. Lougovski, Optica **4**, 8 (2017).
[33] R. C. Miller, Applied Physics Letters **5**, 17 (1964).
[34] A. W. Smith and N. Braslau, Journal of Applied Physics **34**, 2105 (1963).
[35] R. W. Boyd, *Nonlinear optics* (Academic press, 2020).
[36] M. Cazzanelli, F. Bianco, E. Borga, G. Pucker, M. Ghulinyan, E. Degoli, E. Luppi, V. Véniard, S. Ossicini, D. Modotto, *et al.*, Nat. Materials **11**, 148 (2012).
[37] T. Ning, H. Pietarinen, O. Hyvärinen, J. Simonen, G. Genty, and M. Kauranen, Appl. Phys. Lett. **100**, 161902 (2012).
[38] E. Timurdogan, C. V. Poulton, M. Byrd, and M. Watts, Nat. Photonics **11**, 200 (2017).
[39] H. J. McGuinness, M. G. Raymer, C. J. McKinstrie, and S. Radic, Phys. Rev. Lett. **105**, 093604 (2010).
[40] A. S. Clark, S. Shahnia, M. J. Collins, C. Xiong, and B. J. Eggleton, Opt. Lett. **38**, 947 (2013).
[41] Q. Li, M. Davanço, and K. Srinivasan, Nat. Photonics **10**, 406 (2016).
[42] Y. Zhao, D. Lombardo, J. Mathews, and I. Agha, APL Photonics **2**, 026102 (2017).
[43] B. A. Bell, C. Xiong, D. Marpaung, C. J. McKinstrie, and

B. J. Eggleton, Opt. Lett. **42**, 1668 (2017).
[44] X. Lu, Q. Li, D. A. Westly, G. Moille, A. Singh, V. Anant, and K. Srinivasan, Nat. Phys. **15**, 373 (2019).
[45] C. McKinstrie, J. Harvey, S. Radic, and M. Raymer, Opt. Express **13**, 9131 (2005).
[46] K. Saha, Y. Okawachi, O. Kuzucu, M. Menard, M. Lipson, and A. L. Gaeta, in *CLEO: QELS_Fundamental Science* (Optical Society of America, 2013) pp. QF1D–2.
[47] J. Chen, X. Li, and P. Kumar, in *Quantum Communications and Quantum Imaging II*, Vol. 5551 (International Society for Optics and Photonics, 2004) pp. 121–128.
[48] G. P. Agrawal, in *Nonlinear Science at the Dawn of the 21st Century* (Springer, 2000) pp. 195–211.
[49] E. A. Kittlaus, H. Shin, and P. T. Rakich, Nat. Photonics **10**, 463 (2016).
[50] E. A. Kittlaus, N. T. Otterstrom, and P. T. Rakich, Nat. Commun. **8**, 1 (2017).
[51] G. Huang, E. Lucas, J. Liu, A. S. Raja, G. Lihachev, M. L. Gorodetsky, N. J. Engelsen, and T. J. Kippenberg, Phys. Rev. A **99**, 061801 (2019).
[52] N. T. Otterstrom, E. A. Kittlaus, S. Gertler, R. O. Behunin, A. L. Lentine, and P. T. Rakich, Optica **6**, 1117 (2019).
[53] R. Claps, D. Dimitropoulos, Y. Han, and B. Jalali, Opt. Express **10**, 1305 (2002).
[54] J. I. Dadap, R. L. Espinola, R. M. Osgood, S. J. McNab, and Y. A. Vlasov, Opt. Lett. **29**, 2755 (2004).
[55] R. L. Espinola, J. I. Dadap, R. M. Osgood, S. J. McNab, and Y. A. Vlasov, Opt. Express **12**, 3713 (2004).
[56] C. J. McKinstrie, S. Radic, and M. Raymer, Opt. Express **12**, 5037 (2004).
[57] T. Liang and H. Tsang, Appl. Phys. Lett. **85**, 3343 (2004).
[58] The nonreciprocal functionality is preserved provided the pulse is significantly narrower than the phase-matching bandwidth.